TITLE

Low-power-consumption, high-current-density, and propellantless cathode using graphene-oxide-semiconductor structure array

Author names and Affiliations

Ryo Furuya[1,2], Yoshinori Takao[3], Masayoshi Nagao[2], and Katsuhisa Murakami[2,*]

[1]*Department of Mechanical Engineering, Materials Science, and Ocean Engineering, Yokohama National University, Yokohama, 240 – 8501, Japan*

[2]*Device Technology Research Institute, National Institute of Advanced Industrial Science and Technology, Tsukuba, 305 – 8560, Japan*

[3]*Division of Systems Research, Yokohama National University, Yokohama, 240 – 8501, Japan*

* Corresponding author.

TEL/FAX: +81-29-861-4723/+81-29-861-5507

E-mail address: murakami.k@aist.go.jp

Keywords

Microspacecraft

Neutralizer

Graphene-oxide-semiconductor

Electron sources

Electrodynamic tether

ABSTRACT

Graphene-oxide-semiconductor (GOS) planar-type electron sources—which consist of a graphene electrode layer, a thin SiO_2 insulator, and a Si substrate—can be driven by applying gate biases of 5–15 V to produce high emission current densities of 10–100 mA/cm^2. In this study, propellantless cathodes using GOS electron sources are developed for aerospace applications. Because a single emission site usually has an area smaller than 100 μm × 100 μm, its maximum emission current is below 10 μA. To increase the emission current to several milliamperes or more, the total emission area must be expanded. However, it is difficult to increase the emission current by merely enlarging a single emission area because the graphene layer acts not only as the gate electrode but also as a series resistor, which means that the emission current density decreases as the effective gate bias decreases. Thus, the optimum relationship between the area of a single emission site and the emission current of the site array

is investigated, showing a result that an electron source with hundreds of 100 μm × 100 μm sites on a 3 mm × 3 mm wafer produces an emission current of 6.0 mA at a gate bias of 11.1 V.

Nomenclature

AFM	=	Atomic Force Microscopy
BHF	=	Buffered Hydrogen Fluoride
CNTFEC	=	Carbon Nanotude Field-Emission Cathode
CVD	=	Chemical Vapor Deposition
EB	=	Electron-Beam
EDT	=	Electrodynamic Tether
FECs	=	Field-Emission Cathodes
FEN	=	Field-Emission Neutralizer
FN	=	Fowler–Nordheim
GOS	=	Graphene-Oxide-Semiconductor
I_E	=	electron emission current
I_T	=	total current
V_G	=	gate voltage
η	=	emission efficiency

1. INTRODUCTION

In recent years, demand has increased for small spacecraft that use electric propulsion systems so that they can go on space missions frequently and inexpensively, such as for deep space exploration, earth observation, and broadband constellation deployment [1]. For example, ion thrusters have been used because of their high specific impulse and delta-v [2–4]. In ion thrusters, electrons are emitted from neutralizers to the ion beams to prevent spacecraft charging [5–8]. Because the electrons do not contribute to the thrust, the propellant and power consumption of the electron source must be reduced as much as possible to increase the specific impulse or spacecraft payload, especially in microspacecraft with limited power and space. This requirement is also true for electron emitters of electrodynamic tether (EDT) propulsion, an attractive debris removal system [9].

An example of pioneering propellantless electron sources that require no gas flow to perform their functions is field-emission cathodes (FECs), such as CNTFEC and Si FEN [9–14]. Because FECs are field-emission devices based on tunneling, they can emit electrons just by applying an electric field, so that they do not require propellant. Moreover, the power consumption and device size for plasma generation can be reduced using FECs instead of conventional plasma neutralizers. However, conventional FECs are driven at hundreds of volts

because tunneling requires a strong electric field (more than 10^8 V/m) [13,15]. Thus, we have developed a graphene-oxide-semiconductor (GOS) planar-type electron source as a new propellantless cathode, which can be driven at a much lower voltage than other FECs.

The GOS electron source can be driven at a gate bias of 5–15 V, much lower than that of other FECs, typically 200 V or more. Moreover, the emission current density—the emission current divided by the emission area—of the GOS electron source is 10–100 mA/cm^2 [16–18], which is two to three orders of magnitude higher than those of other FECs.

As shown in Fig. 1(a), the GOS electron source mainly consists of four materials: n-type Si as a substrate, thin SiO_2 as an insulating layer, 1–1.4 nm graphene (3 to 4 layers of graphene) as an upper electrode layer, and Ni/Ti as a contact electrode. By applying a gate bias between the Si substrate and the contact electrode on the graphene, electrons accumulate between the insulating layer and the Si substrate. By increasing the gate bias, the potential barrier of the insulating layer decreases in width. When the electric field in the insulating layer becomes high enough to enable tunneling, electrons pass through the insulating layer. Transmitted electrons with energy higher than the work function of the graphene electrode are emitted into vacuum through the graphene electrode. The other transmitted electrons flow to the contact electrode as the gate current.

Let the ratio of the electron emission current to the total current (the sum of the electron emission current and gate current) through the insulating layer be the emission efficiency. To improve the emission efficiency, the inelastic electron scattering cross-section in the upper electrode should be small. Moreover, the upper electrode should be as thin as possible so that electrons can pass through it.

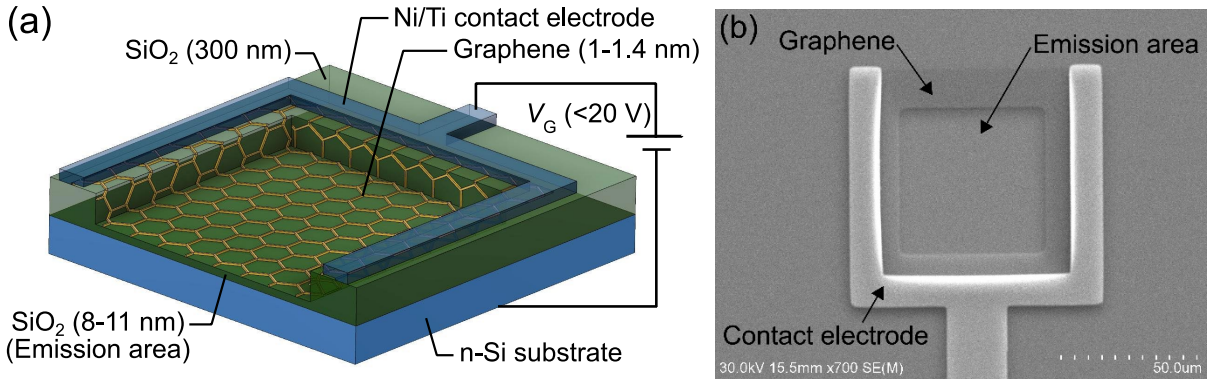

Fig. 1. Electron sources based on the graphene-oxide-semiconductor structure. (a) A schematic, where an U-shaped dark blue layer is a contact electrode composed of Ni and Ti, a hexagonal yellow layer is an upper graphene electrode layer, a green layer is a SiO_2 insulating layer, and a bright blue layer under the SiO_2 is a Si substrate. (b) Scanning electron microscopy image of a 50 μm × 50 μm emission area.

Graphene is a two-dimensional monolayer carbon material with a small inelastic scattering cross-section. Thus, GOS electron sources have shown an emission efficiency of 10–30% [19–20], much higher than those of conventional metal–oxide–semiconductor electron

sources (0.01% or less) [21–24]. However, GOS electron sources only produce emission currents of several tens of microamperes because of their small emission area, currently up to 100 μm × 100 μm. To achieve an emission current of several milliamperes, matching that of conventional FECs, we have worked to expand the emission area of the GOS electron source.

The emission area can be expanded in two ways: by expanding a single emission site or by fabricating an array of tiny emission sites. It may seem easy to increase the emission current in these ways, but the emission current density decreases as the emission area increases, because the effective voltage in the emission area decreases from the sheet resistance of the graphene electrode. Moreover, contact electrodes surround each emission area, as shown in Fig. 1(b), so that adding more emission sites will decrease the effective emission area. Thus, in this paper, we worked to optimize the relationship between the emission area and array pattern. By doing so, we produced a GOS electron source with an emission current of a few milliamperes, with better emission current density and lower cost than other FECs and miniature plasma neutralizers.

2. EXPERIMENT

Fig. 2 shows the procedure for fabricating the GOS electron sources, detailed as follows. The pattern of the emission area was formed on an n-Si substrate by etching 300-nm SiO_2 on

the n-Si by using buffered hydrogen fluoride (BHF). Then, thin SiO_2 (8–11 nm) was grown on the n-Si substrate by oxidizing the surface of the n-Si at 900 °C under oxygen gas flow of 1 L/min at atmospheric pressure. Next, 1.4 nm graphene was directly synthesized on the SiO_2 by chemical vapor deposition (CVD). After the graphene layer was partially etched by oxygen plasma ashing, Ni and Ti were deposited on the top and bottom of the wafer by using electron-beam (EB) vacuum evaporation.

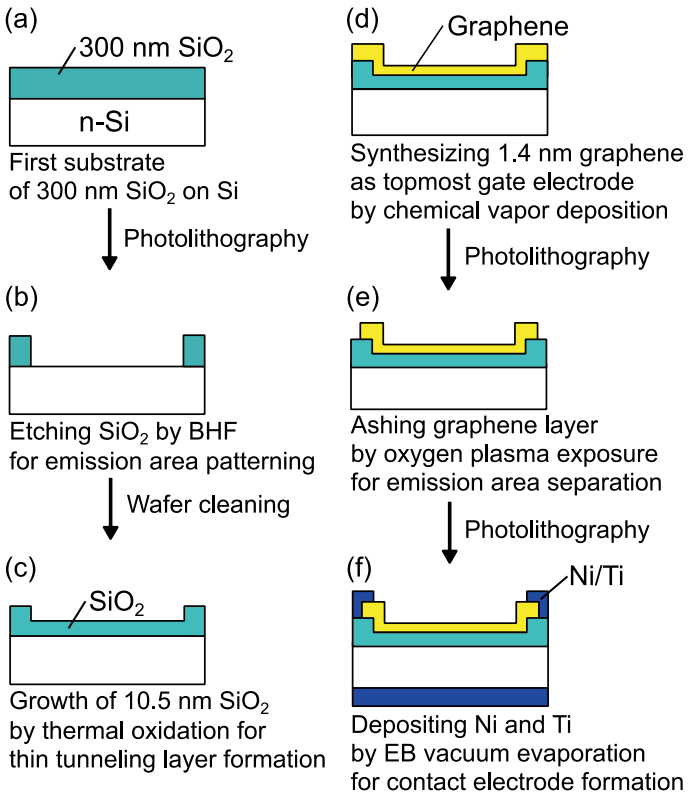

Fig. 2. Fabrication process of the graphene-oxide-semiconductor electron source.

Notably, thinning the SiO_2 insulating layer increases the emission current because it increases the transmission of electrons. However, it also increases the probability of defects, which are caused by damage to the SiO_2 during graphene synthesis. These defects cause a short circuit in the insulating layer, producing a leakage current and deactivating an emission area. In this paper, we used 10.5 nm of SiO_2 as the standard thickness of the electron source based on previous experiments [20].

Fig. 3 shows a schematic of the experimental setup. The emission performance of the electron source is measured in a vacuum chamber at 1.0×10^{-6} Pa. When a gate bias V_G of 0–15 V at intervals of 0.1 V is applied by a Keithley 236 Source Measure Unit, electrons are emitted and encounter the stainless-steel collector plate, where the n-Si substrate via the back side Ni/Ti contact layer was also connected to another Keithley 236 Source Measure Unit and the collector plate was biased at 1 kV by a Keithley 237 High Voltage Source Measure Unit to avoid space-charge limitation. The electron emission current I_E in the collector and the total current I_T in the n-Si substrate are measured. The emission characteristics are evaluated from the emission current density J, described as $J = I/S$, where I is the current (I_E or I_T) and S is the total emission area, and the emission efficiency η is described as $\eta = I_E / I_T$. Note that these Source Measure Units have an accuracy below ±0.04%.

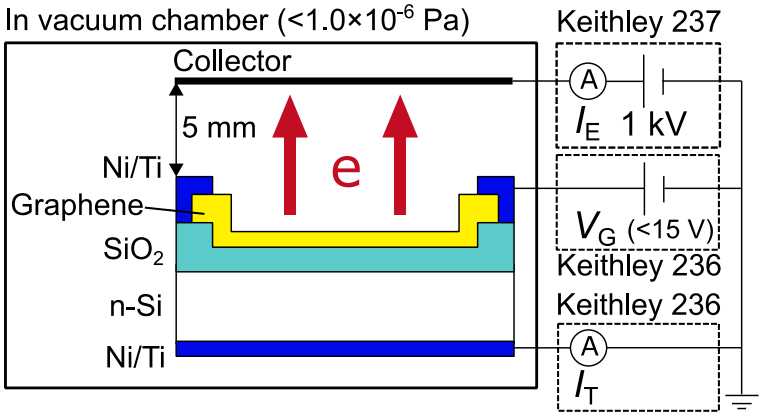

Fig. 3. Circuit diagram of the current measurements of the graphene-oxide-semiconductor electron source.

The Fowler–Nordheim (FN) equation gives the transmitted electron current I through the insulating layer as

$$I = \frac{S\beta^2 e^3}{8\pi h\phi d^2} V^2 exp\left(-\frac{8\pi d\phi^{3/2}\sqrt{2m_e}}{3eh\beta}\cdot\frac{1}{V}\right) \quad (1)$$

where V is the applied voltage, S is the emission area, β is a field enhancement factor, e is the elementary positive charge, h is Planck's constant, ϕ is the work function of the emission area, d is the separation distance, and m_e is the electron mass [25]. Here, taking the natural logarithm of both sides of Eq. (1) gives

$$\ln(I/V^2) = \mathrm{B}/V + \ln \mathrm{A} \quad (2)$$

where the coefficient of V^2 and $1/V$ are replaced with A and B. In Eq. (2), $\ln \mathrm{A}$ and B are the intercept and slope, respectively, of the fit line of the FN plot. The electron emission of the FN tunneling can be detected by linearizing the transmitted electron current using the FN plot.

Moreover, an ideal FN tunneling curve can be plotted in the *I–V* curves, assigning the intercept and slope of the fitted line of the FN plot to Eq. (2). The tunneling characteristics of the GOS electron source were evaluated by comparing the measured *J–V* characteristics and the FN tunneling curve of the total current using the FN plots.

3. RESULTS AND DISCUSSION

To fabricate the array of tiny emission sites, we assessed the relationship between the emission current density in a single emission site and the emission area. To assess this, we fabricated various emission sites and evaluated their emission performance. Then, we designed an array in a 3 mm × 3 mm area, composed of hundreds of small emission sites that can be driven with high emission current density. After estimating the maximum emission current from this array, we fabricated an electron source using this array and measured its emission performance.

3.1. Emission performance of a single emission site

We evaluated the emission performance from the *J–V* characteristics of a single emission site—with an area of 50 μm × 50 μm, 100 μm × 100 μm, or 200 μm × 200 μm—by applying a gate bias up to 15 V. Fig. 4 shows the *J–V* characteristics of GOS electron sources

with three different emission areas and an 10.5-nm-thick insulating layer, as well as the FN tunneling current obtained from the linear fit of the total current in the FN plot (FN fitting).

As shown in Fig. 4(a), the electron source with a single 50 μm × 50 μm emission site maintained an emission efficiency of over 20% in the range of 8.0–11.5 V and achieved a maximum emission current density of 230 mA/cm^2 at 14.1 V. As shown in Fig. 4(b), the emission efficiency of over 20% was maintained in 7.5–13.9 V, and the maximum emission current density was 184 mA/cm^2 from 100 μm × 100 μm area, and in Fig. 4(c), over 20% was maintained in 7.3–14.0 V and 118 mA/cm^2 was obtained from the 200 μm × 200 μm area. The highest emission current density was achieved by a 50 μm × 50 μm area at a gate bias of 14.1 V. Additionally, the emission current density of these electron sources dropped at the gate bias over 14.1 V, indicating that the electric breakdown in the insulating layer occurred and the emission efficiency decreased owing to an increase of leakage current.

In the FN plot, the total current represents the straight lines in a range corresponding to a gate bias of 8–10 V, which implies that the electrons transmitted through the insulating layer by optimal FN tunneling. However, in the *J*–*V* curves, the slope of the total current density for each emission area appears to decrease at a gate bias of ~10.5 V compared with the FN fitting curve. The decrease in total current indicates that the effective electrical potential to the emission area drops by the graphene sheet resistance near a gate bias of 10 V or more.

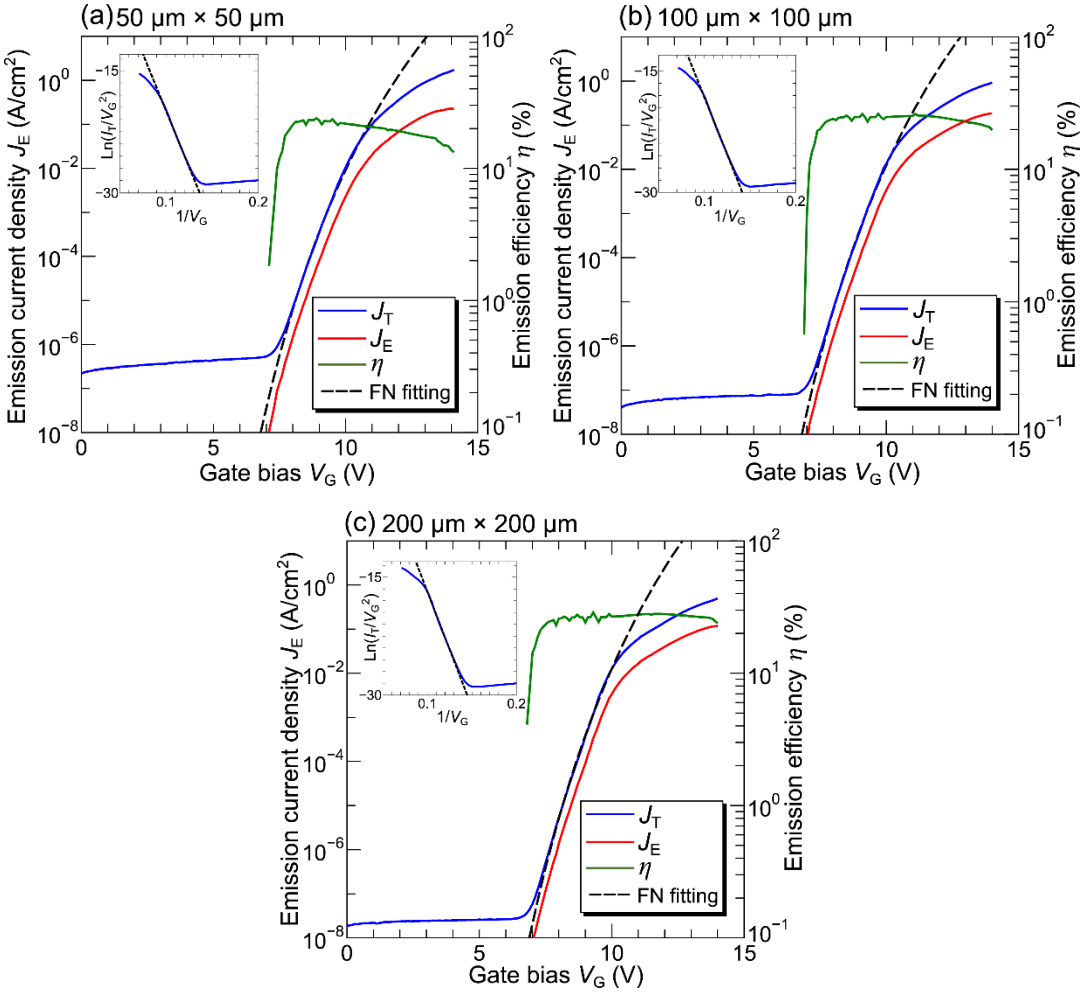

Fig. 4. The total current density J_T, the emission current density J_E, and the emission efficiency η of the graphene-oxide-semiconductor electron sources with a single emission site as a function of gate bias V_G, where the SiO_2 thickness was 10.5 nm and the vacuum pressure for the electron emission measurement was 1.0×10^{-6} Pa. The insets show the I–V dependence on the Fowler–Nordheim (FN) plots and its liner fitting. (a) 50 μm × 50 μm, (b) 100 μm × 100 μm, and (c) 200 μm × 200 μm emission sites.

Fig. 5 shows the emission current density for each emission area at a gate bias of 9–15 V. The emission current density among the emission area at a gate bias of 14 V is much different from that at 10 V. Moreover, the emission current density increases as the emission area decreases because the effective gate bias in the emission area decreases owing to the sheet resistance of the graphene electrode, where it was determined to be 1.0×10^5 Ω/square in this series. For the total current of 93 μA in the 100 μm × 100 μm emission area at a gate bias of 14 V, the effective gate bias in the middle of the emission area (50 μm away from the contact electrode) is 9.3 V, which decreases the electron emission current density. Thus, the emission area clustered must be as small as possible to increase the emission current density. Additionally, the effect of defects inhibiting electron emission for an entire emission site can be kept in a tiny area by clustering the small emission sites.

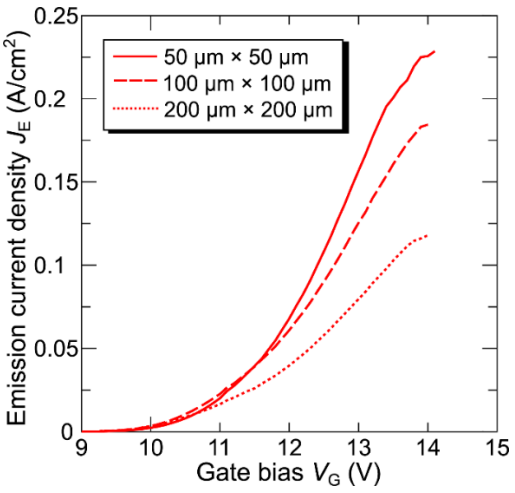

Fig. 5. The emission current density J_E of graphene-oxide-semiconductor electron sources with three different single emission sites at gate biases of 9–15 V.

3.2. Emission performance with massive emission sites

The array patterns of massive emission sites were designed on a 3 mm × 3 mm wafer. The total emission area is 3.8 mm^2 for 380 sites of 100 μm × 100 μm and 2.1 mm^2 for 840 sites of 50 μm × 50 μm. From the maximum emission current density as shown in Fig. 4 and the total emission area for each array pattern, the estimated maximum emission current is 4.8 mA for the array of 50 μm × 50 μm area and 7.0 mA for the array of 100 μm × 100 μm area. The array of 100 μm × 100 μm area is preferable to maximize emission current. However, the array of 50 μm × 50 μm has many more emission sites than the array of 100 μm × 100 μm and can reduce the effect of defects. Thus, both the 50 μm × 50 μm and 100 μm × 100 μm arrays were fabricated. Optical microscopy images of the 100 μm × 100 μm array (referred to as Array-100 pattern) and the 50 μm × 50 μm array (Array-50 pattern) are shown in Fig. 6(a) and 6(b), respectively. In these arrays, a positive potential is applied to each emission site via the comb-like contact electrodes surrounding each emission site with a U-shaped electrode.

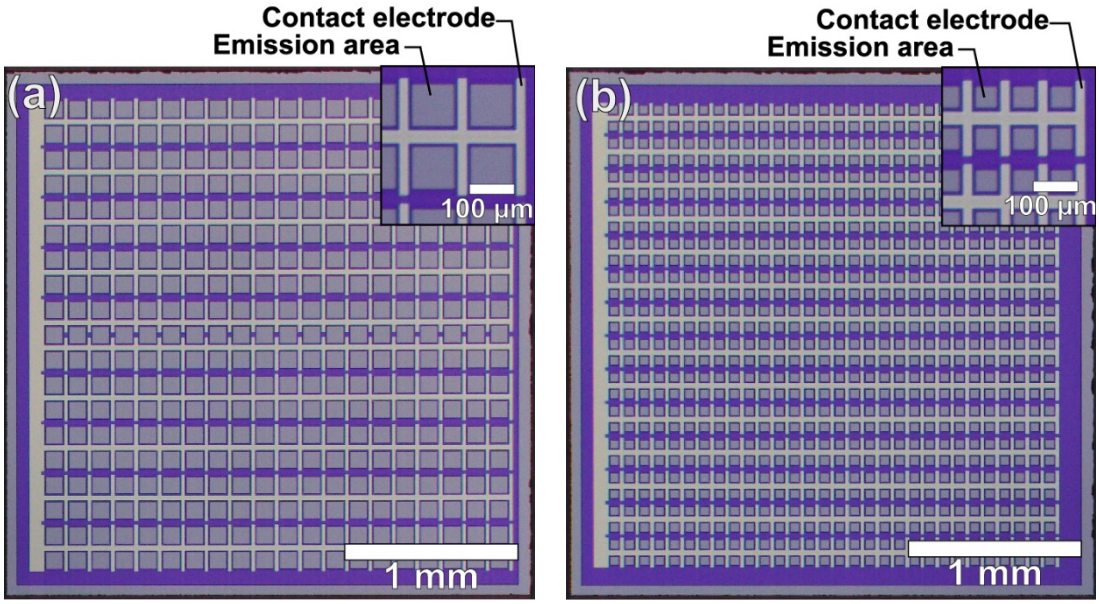

Fig. 6. Optical microscopy images of the graphene-oxide-semiconductor electron sources. (a) Array of 100 μm × 100 μm area (referred to as Array-100 pattern). (b) Array of 50 μm × 50 μm area (referred to as Array-50 pattern). The insets show magnified views around the emission areas.

Fig. 7 shows the *I*–*V* characteristics of the electron sources with an array of massive emission sites. The emission performance is evaluated at gate biases of 0–15 V. In the Array-100 pattern with 10.5-nm SiO_2 shown in Fig. 7(a), the electron source started emitting at a gate bias of 6.3 V. As the gate bias increased, it maintained a high emission efficiency of 10–30% in the range of 9.4–13.4 V and reached a maximum emission current of 2.1 mA at 13.4 V. The

measured emission current was smaller than the estimate of 7.0 mA. Thus, we tried to increase the emission current of the electron source by thinning the SiO_2.

An Array-100 pattern electron source with 8.5-nm SiO_2 was fabricated, and its emission characteristics were evaluated. As shown in Fig. 7(b), electrons were emitted at a gate bias of 4.1 V, and the emission efficiency of 10–22% was maintained in the range of 8.9–11.5 V. A maximum emission current of 6.0 mA was achieved at 11.1 V. However, its maximum emission efficiency (22%) was lower than that of the 10.5-nm SiO_2 layer (30%). This result was probably caused by the increase in leakage current owing to the thinner insulating layer. The Array-100 pattern with a 8.5-nm SiO_2 layer achieved higher total current at lower gate bias voltage than that with the 10.5-nm SiO_2 layer, implying that defects were likely to emerge in the thinner insulating layer, increasing the leakage current. Finally, the Array-100 pattern electron source was driven with an emission current near the estimated value, and we demonstrated a mA-class cathode using the GOS electron source with the Array-100 pattern.

Fig. 7(c) shows the emission characteristics of the electron source with the Array-50 pattern. Its maximum emission current was 22 μA at 15.0 V, which is two orders of magnitude lower than that of the Array-100 pattern. The sheet resistance of the graphene electrode was 4.5 MΩ/square in the Array-50 pattern, which is higher than that of 0.1–0.4 MΩ/sq. in the Array-100 pattern. Thus, the effective gate bias in the Array-50 pattern was suppressed by the high

resistance of the graphene electrode, lowering the transmitted electron current. However, the emission efficiency of the Array-50 pattern (32%) was higher than that of Array-100, indicating that the graphene electrode in Array-50 was thinner than that in Array-100. A thin graphene electrode increases the emission efficiency from the surface of the graphene, contrasting its high sheet resistance that restricts electron transmission through the insulating layer.

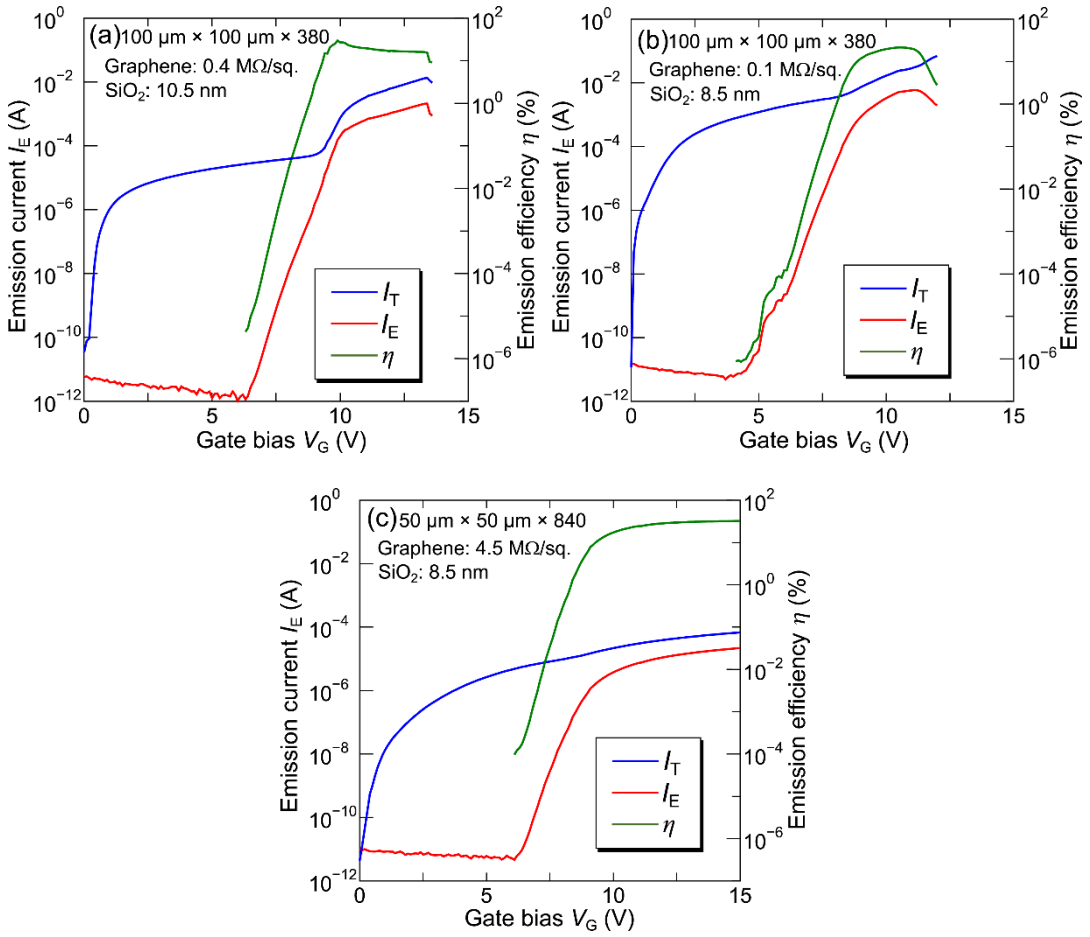

Fig. 7. The total current I_T, the emission current I_E, and the emission efficiency η of the graphene-oxide-semiconductor electron sources as a function of gate bias V_G, where the vacuum pressure at the electron emission measurement was 1.0×10^{-6} Pa. (a) Array of 100 μm × 100

μm area with 10.5 nm SiO_2. (b) Array of 100 μm × 100 μm area with 8.5 nm SiO_2. (c) Array of 50 μm × 50 μm area with 8.5 nm SiO_2.

As shown in Fig. 7, leakage current emerged at low gate biases of 0–5 V in these three electron sources with array patterns. Fig. 8 shows a conductive atomic force microscopy (AFM) image between an emission site and the 300-nm SiO_2 layer. The electric field is locally enhanced at the edge of the emission site, where the SiO_2 thickness changes from 300 nm to 10 nm, and electric breakdown tends to occur, producing leakage current there. Here, the total edge length of 168 mm in Array-50 is longer than that of 152 mm in Array-100. Thus, the Array-100 pattern tends to have fewer leakage sites than in Array-50. In our future work, we will develop an array of emission sites that have a series resistance of graphene between the contact electrode and each emission site to suppress the overcurrent caused by defects.

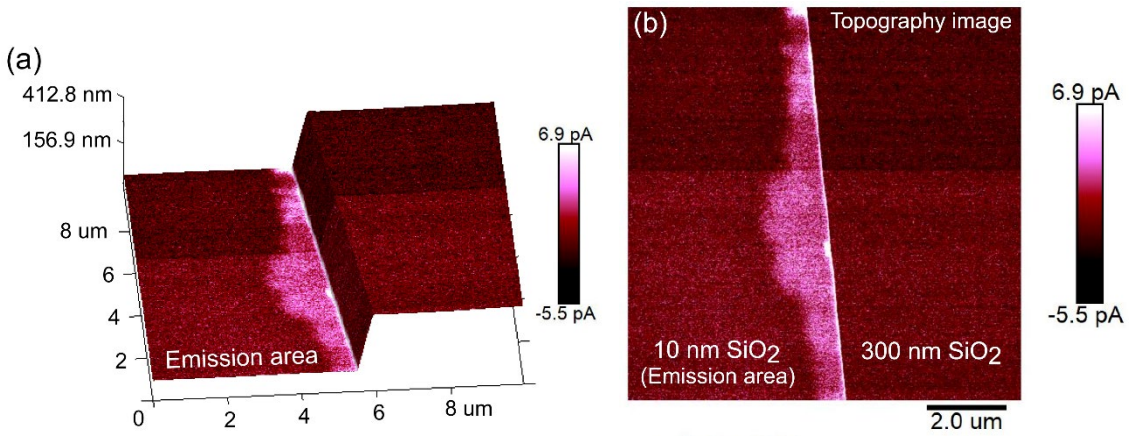

Fig. 8. Conductive atomic force microscopy (AFM) images between the emission area and the 300-nm SiO_2 of a graphene-oxide-semiconductor electron source. The high current domain in the emission area represents a leakage current area where the electrons are not emitted in vacuum. (a) A three-dimensional (3D) topography image with wafer height. (b) A two-dimensional (2D) topography image on the surface of the electron source.

Finally, the emission performances are compared between the GOS electron source with the Array-100 pattern, which achieved a maximum emission current of 6.0 mA, and other mA-class electron sources. Table 1 compares the emission current, current density, and cost of the GOS electron sources, conventional FECs (Si FEN [12] and CNTFEC [10]), and a miniature plasma neutralizer (BRFC-1 [5]). Here, the emission current density is assessed from the emission current at each device size: 3 mm × 3 mm of GOS electron sources, 6 mm × 6 mm of Si FEN, 88 mm × 88 mm of CNTFEC, and 10 mm in diameter of BRFC-1. Also, the electron emission cost is calculated from the input power required to emit electrons divided by the emission current. As shown in the table, the emission current density to the device size of the GOS electron sources is 66.7 mA/cm^2, which is ten times higher than that of conventional FECs. Moreover, the electron emission cost of the GOS electron sources is 57 W/A, which is the lowest cost among the mA-class electron sources referenced in this paper. In conclusion, our

GOS electron source is superior to the other mA-class electron sources in emission density and power consumption, where it would contribute to reducing power consumption and the propellant storage of a neutralizer for micro ion thrusters and electron-emitting devices for an EDT propulsion system.

Table 1. Emission current, current density, and cost of the GOS electron sources compared with conventional FECs and a miniature plasma neutralizer. The values of CNTFEC, Si FEN, and BRFC-1 are calculated from the references listed.

	Emission current [mA]	Emission current density [mA/cm^2]	Electron emission cost [W/A]	Reference
GOS	6.0	67	57	-
CNTFEC	3.0	0.04	320	10
Si FEN	1.0	2.8	127	12
BRFC-1	10	3.2	1100	5

4. CONCLUSION

We proposed graphene-oxide-semiconductor (GOS) planar-type electron sources as promising propellantless low-voltage-driven cathodes for electric propulsion systems used in space. To obtain an emission current of several milliamperes, we fabricated electron sources with an array of small emission sites. First, we investigated the emission performance from a single emission site. From the relationship between the emission current density and effective

bias degradation due to the graphene sheet resistance, we chose 100 μm × 100 μm as the optimal emission area to be clustered. Next, we fabricated electron sources with an array of 380 sites, each with an area of 100 μm × 100 μm, on a 3 mm × 3 mm wafer. The electron source achieved a maximum emission current of 6.0 mA at a gate bias of 11.1 V. Moreover, its emission current density of 66.7 mA/cm^2 and electron emission cost of 57 W/A are much better than those of other mA-class electron sources. Overall, we demonstrated GOS electron sources that achieve emission of a few milliamperes, which can be used as neutralizers of miniature ion thrusters and as electron emitters of electrodynamic tethers.

ACKNOWLEDGMENTS

This work was partly supported by JSPS KAKENHI (Grant Numbers JP18H01505 and JP18K18910) and the JAXA Research and Development Directorate, Japan.

REFERENCES

[1] T. Wekerle, J.B. Pessoa Filho, L.E.V.L. Da Costa, L.G. Trabasso, Status and Trends of Smallsats and their Launch Vehicles - An up-to-date Review, J. Aerosp. Technol. Manag. 7 (2017) 269–286. http://dx.doi.org/10.5028/jatm.v9i3.853

[2] S. Yoshimoto, S. Nakasuka, Y. Tsuruda, Y. Aoyanagi, T. Tanaka, H. Sahara, T. Ohira, Y. Araki, I. Mase, M. Ito, V. Kainov, A. Karandaev, O. Silkin, Cluster Launch of Hodoyoshi-3 and -4 Satellites from Yasny by Dnepr Launch Vehicle, Trans. Jpn. Soc. Aeronaut. Space Sci., Aerosp. Technol. Jpn. 14 (2016) Pf_35–Pf_43. https://doi.org/10.2322/tastj.14.Pf_35

[3] H. Koizumi, H. Kawahara, K. Yaginuma, J. Asakawa, Y. Nakagawa, Y. Nakamura, S. Kojima, T. Matsuguma, R. Funase, J. Nakatsuka, K. Komurosaki, Initial Flight Operations of the Miniature Propulsion System Installed on Small Space Probe: PROCYON, Trans. Jpn. Soc. Aeronaut. Space Sci., Aerosp. Technol. Jpn. 14 (2016) Pb_13–Pb_22. https://doi.org/10.2322/tastj.14.Pb_13

[4] B.K. Malphrus, K.Z. Brown, J. Garcia, C. Conner, J. Kruth, M.S. Combs, N. Fite, S. McNeil, S. Wilczweski, K. Haught, A. Zucherman, P. Clark, K. Angkasa, N. Richard, T. Hurford, D. Folta, C. Brambora, R. MacDowall, P. Mason, S. Hur-Diaz, J. Breeden, R. Nakamura, A. Martinez, M.M. Tsay, The Lunar IceCube EM-1 Mission: Prospecting the Moon for Water Ice, IEEE Aerosp. Electron. Syst. Mag. 34 (2019) 6–14. https://doi.org/10.1109/MAES.2019.2909384

[5] M. Tsay, J. Frongillo, J. Model, J. Zwahlen, L. Paritsky, Maturation of Iodine-Fueled BIT-3 RF Ion Thruster and RF Neutralizer, in: 52nd AIAA, SAE/ASEE Joint Propulsion Conference, 2016, AIAA 2016-4544. https://doi.org/10.2514/6.2016-4544

[6] H. Masui, Y. Tashiro, N. Yamamoto, H. Nakashima, I. Funaki, Analysis of Electron and Microwave Behavior in Microwave Discharge Neutralizer, Trans. Japan Soc. Aero. Space Sci. 49 (2006) 87–93. https://doi.org/10.2322/tjsass.49.87

[7] M.D. Goebel, M.R. Watkins, K.K. Jameson, LaB_6 Hollow Cathodes for Ion and Hall Thrusters, J. Propul. Power 23 (2007) 552–558. https://doi.org/10.2514/1.25475

[8] H. Koizumi, K. Komurasaki, J. Aoyama, K. Yamaguchi, Development and Flight Operation of a Miniature Ion Propulsion System, J. Propul. Power 34 (2017) 960–968. https://doi.org/10.2514/1.B36459

[9] Y. Okawa, S. Kitamura, S. Kawamoto, Y. Iseki, K. Hashimoto, E. Noda, An experimental study on carbon nanotube cathodes for electrodynamic tether propulsion, Acta Astronaut. 61 (2007) 989–994. https://doi.org/10.1016/j.actaastro.2006.12.017

[10] N. Yamamoto, T. Morita, Y. Ohkawa, M. Nakano, I. Funaki, Ion Thruster Operation with Carbon Nanotube Field Emission Cathode, J. Propul. Power 35 (2019) 490–493. https://doi.org/10.2514/1.B37214

[11] C.J. Gasdaska, P.Falkos, V. Hruby, M. Robin, N. Demmons, R. McCormick, D. Spence, J. Young, “Testing of Carbon Nanotube Field Emission Cathodes, in: 40th AIAA/ASME/SAE/ASEE Joint Propulsion Conference and Exhibit, 2004, AIAA 2004-3427. https://doi.org/10.2514/6.2004-3427

[12] A.A. Fomani, A.I. Akinwande, L. F. Velásquez-García, Resilient, Nanostructured, High-Current, and Low-Voltage Neutralizers for Electric Propulsion of Small Spacecraft in Low Earth Orbit, J. Phys.: Conf. Ser. 476 (2013) 012014. https://doi.org/10.1088/1742-6596/476/1/012014

[13] K.L. Aplina, B.J. Kenta, W. Songb, C. Castellic, Field emission performance of multiwalled carbon nanotubes for a low-power spacecraft neutraliser, Acta Astronaut. 64 (2009) 875–881. https://doi.org/10.1016/j.actaastro.2008.10.012

[14] J.M. Makela, R.L. Washeleski, L.B. King, Regenerable Field Emission Cathode for Spacecraft Neutralization, J. Propul. Power 25 (2009) 970–975. https://doi.org/10.2514/1.41541

[15] I. Brodie, C.A. Spindt, Vacuum microelectronics, Adv. Electron. Electron Phys. 83 (1992) 1–106. https://doi.org/10.1016/S0065-2539(08)60006-2

[16] K. Murakami, S. Tanaka, A. Miyashita, M. Nagao, Y. Nemoto, M. Takeguchi, J. Fujita, Graphene-oxide-semiconductor planar-type electron emission device, Appl. Phys. Lett. 108 (2016) 083506. https://doi.org/10.1063/1.4942885

[17] K. Murakami, M. Nagao, T. Iijima, Y. Yamada, M. Sasaki, Y. Nemoto, M. Takeguchi, Annealing effect on electron emission properties of graphene-oxide-semiconductor planar-

type electron emission devices, in: 30st International Vacuum Nanoelectronics Conference, 2017, FEC-P01. https://doi.org/10.1109/IVNC.2017.8051568

[18] K. Murakami, S. Tanaka, T. Iijima, M. Nagao, Y. Nemoto, M. Takeguchi, Y. Yamada, M. Sasaki, Electron emission properties of graphene-oxide-semiconductor planar-type electron emission devices, J. Vac. Sci. Technol. B 36 (2018) 02C110. https://doi.org/10.1116/1.5006866

[19] K. Murakami, J. Miyaji, R. Furuya, M. Adachi, M. Nagao, Y. Neo, Y. Takao, Y. Yamada, M. Sasaki, H. Mimura, High-performance planar-type electron source based on a graphene-oxide-semiconductor structure, Appl. Phys. Lett. 114 (2019) 213501. https://doi.org/10.1063/1.5091585

[20] R. Furuya, K. Murakami, M. Nagao, Y. Takao, Improvement of Electron Emission Efficiency of Graphene-Oxide-Semiconductor Planar-Type Electron Sources for Nanosatellite Neutralizers, in: 31st International Vacuum Nanoelectronics Conference, 2018, P1-43. https://doi.org/10.1109/IVNC.2018.8519982

[21] S.H. Lo, D.A. Buchanan, Y. Taur, W. Wang, Quantum-Mechanical Modeling of Electron Tunneling Current from the Inversion Layer of Ultra-Thin-Oxide nMOSFET's, IEEE Electr. Device Lett. 18 (1997) 209–211. https://doi.org/10.1109/55.568766

[22] K. Yokoo, H. Tanaka, S. Sato, J. Murota, S. Ono, Emission characteristics of metal–oxide–semiconductor electron tunneling cathode, J. Vac. Sci. Technol. B 11 (1993) 429–432. https://doi.org/10.1116/1.586877

[23] K. Yokoo, G. Koshita, S. Hanzawa, Y. Abe, Y. Neo, Experiments of highly emissive metal–oxide–semiconductor electron tunneling cathode, J. Vac. Sci. Technol. B 14 (1996) 2096–2099. https://doi.org/10.1116/1.588878

[24] H. Mimura, Y. Abe, J. Ikeda, K. Tahara, Y. Neo, H. Shimawaki, and K. Yokoo, Resonant Fowler–Nordheim tunneling emission from metal-oxide-semiconductor cathodes, J. Vac. Sci. Technol. B 16 (1998) 803–806. https://doi.org/10.1116/1.589909

[25] R.G. Forbes, Field emission: New theory for the derivation of emission area from a Fowler–Nordheim plot, J. Vac. Sci. Technol. B 17 (1999) 526–553. https://doi.org/10.1116/1.590588